An Experimental Study of 2.4 GHz LoRa in Air-to-Ground Communication

Néstor J. Hernández Marcano*, Christoffer Gjedsted Brask†, Liping Shi*, Rune Hylsberg Jacobsen*
*DIGIT, Department of Electrical and Computer Engineering, Aarhus University, Denmark. {nh|liping|rhj}@ece.au.dk
†Develco A/S, Aarhus, Denmark. cgb@develco.dk

***Abstract*—Channel modeling in radio communication is crucial, especially for emerging technologies like LoRa. While LoRa shows promise for Unmanned Aerial Vehicle (UAV) telemetry and C2 channels, its progress in sub-GHz bands is hindered by duty cycle limitations. LoRa operating at 2.4 GHz has no such restrictions and can achieve higher data rates. However, the propagation characteristics and goodput performance of 2.4 GHz LoRa have not been well studied. In this work, we present path loss, round-trip time, and goodput measurements for air-to-ground communications (A2G) with 2.4 GHz LoRa. We compare our observations with well-known path loss models and find that our measurements are best modeled by the Walfisch-Bertoni model in most cases. Our results demonstrate that for spreading factors SF=7 and SF=10 a link latency of less than 50 ms can be achieved, but it fails to meet the minimum required data rate required for a Command and Control (C2) link.**

***Index Terms*—Unmanned Aerial Vehicle, UAV, Air-to-ground communication, LoRa, wireless channel characterization**

I. Introduction

Recent advances in industrial automation have shown promising development for the use of UAVs for civil infrastructure inspections [1]. For these scenarios, automated and continuous inspections with UAVs allow for a comprehensive solution that mitigates tedious or hazardous human activities [2]. To guide UAVs, reliable communication channels for telemetry and C2 are required.

The European Union Aviation Safety Agency (EASA) has developed a framework in the European Union (EU) covering the regulation of civil Unmanned Aerial Systems [3]. UAVs complying with the regulations must implement a reliable communication link to control all UAVs of a group. In addition, UAVs should be equipped with an automatic link recovery function in case any UAV in the group loses connection with its neighbors or the Ground Control Station (GCS). The maximum average (link) latency should be less than 50 ms for C2 and a guaranteed minimum data rate should be above 60 kbps at the application layer. Furthermore, the uplink should support up to 50 Mbps for mission data with a Packet Loss Rate (PLR) of less than 10^{-3}. This latter requirement cannot be satisfied with LoRa technology. Nevertheless, the requirements for data rates for the telemetry channel are more relaxed assuming values down to a minimum of 0.55 kbps for a single UAV [4].

Long Range (LoRa) offers wide coverage for energy-constrained devices. It operates in the unlicensed Industrial, Scientific, and Medical (ISM) bands, enabling rapid deployment and market adoption. In Europe, sub-GHz bands around 433 MHz and $863 - 870$ MHz have been assigned. LoRa defines the Physical Layer (PHY) aspects of the protocol stack, whereas LoRaWAN addresses higher protocol layers. The radio uses Chirp Spread Spectrum (CSS) modulation, where a narrow-band signal is modulated with a frequency-sweep signal known as a chirp [5]. LoRa trades off throughput for longer ranges by increasing the symbol spread of the modulated signal, leading to an increased time-on-air. LoRa is subjected to duty-cycle regulations of $0.1 - 1\%$ in the sub-GHz ISM bands [6], thus diminishing the average throughput.

In 2018, Semtech released a new LoRa radio chip on the market operating in the 2.4 GHz ISM band [7], which circumvents the duty-cycle limitation. Furthermore, it offers higher data rates than its sub-GHz alternatives, while maintaining the same range by using Spreading Factors (SFs) ranging from 5 to 12, and a communication bandwidth of $BW \in \{203, 406, 812, 1625\}$ kHz. Such developments raise the question of the potential of using LoRa for reliable telemetry and C2 links for UAV applications.

To answer this question, we study Air-to-Ground (A2G) communications with LoRa. Our study is based on the SX1280 radio chip from Semtech supporting operation in the 2.4 GHz frequency band. The key contributions of our work can be summarized as follows:

- We provide path loss and Round Trip Time (RTT) measurements for the A2G link using LoRa at 2.4 GHz.
- We compare the path loss data with conventional path loss models.
- We estimate the RTT distribution and the goodput for the LoRa A2G link based on our measurements.

The experimental setting supports measurements at various distances, UAV altitudes, and SFs representing inspection scenarios in suburban areas.

II. Related work

Most studies of propagation characteristics of LoRa so far have been dedicated to communication operating at sub-GHz frequencies [8], [9]. However, these are not directly applicable to 2.4 GHz LoRa because of their different characteristics e.g., allocated bandwidth, duty-cycle limitations, and SFs range.

Studies of channel models in the 2.4 GHz frequency range include work of [10]–[13]. Kurt and Tavli [13] conducted a review of path-loss models for Wireless Sensor Networks (WSNs) at 868 MHz, 2400 MHz, and 3500 MHz, covering free-space, two-ray, log-distance, and shadowing mod-

els. Khawaja et al. [10] provided a review of air-to-ground propagation channels. In [11], the authors studied the height-dependent multipath propagation due to reflections on the ground and the antenna orientation based on the IEEE 802.11 wireless channel. In [12], the authors reported on an empirical study of the aerial wireless link. They characterized the antenna orientation and the path loss using ZigBee communication (2480 MHz) with UAVs at different heights (1.4 m to 10 m). The free space model and two-ray ground-reflection model were applied as references for the experimental observations.

A few studies have reported on the propagation characteristics of 2.4 GHz LoRa. Zhang et al. [14] considered aquatic environmental monitoring scenarios using 2.4 GHz LoRa. The study addressed Line-of-Sight (LOS), obstructed LOS, and Non-Line-of-Sight (NLOS) using different sets of LoRa parameters. The experimental study focused on Packet Delivery Ratio (PDR) and Received Signal Strength Indicator (RSSI) measurements at different heights from 1 m to 3.5 m above the water level with a range of up to 2700 m. It was concluded that RSSI is a promising indicator for values above a certain sensitivity threshold.

Operation in the 2.4 GHz ISM band is usually jeopardized by interference and noise since it is populated by several wireless technologies such as WiFi and Bluetooth. Polak et al. [15], conducted a performance analysis of the LoRa radio signals interfered by WiFi. The authors used a simulated LoRa band signal and guided propagation in their setup (i.e., no air coupling). Chen et al. [16] proposed a weak signal detection approach to enable the coexistence of LoRa and WiFi.

Higher carrier frequencies and increased bandwidth typically result in a reduced transmission range. In [17], the authors simulated the range capabilities of 2.4 GHz LoRa networks in urban environments. The work implemented the ECC33 path loss model, which is an extension of the Okumura-Hata model. A maximum range of up to 1.13 km for a network of 360 nodes was reported. This result seems far from the theoretical upper limit of 133 km for LoRa 2.4 GHz reported in [18]. Other recent studies of 2.4 GHz LoRa include Time-of-Flight (ToF) ranging [19], [20]. Andersen et al. [19] studied the ranging capabilities of 2.4 GHz LoRa aiming to determine the LoRa parameters that minimize estimation error. Wolf et al. [20], compared a proof-of-concept implementation for coherent multi-channel ranging with narrowband signals to the ToF ranging function of the LoRa 2.4 GHz radio.

Although several studies have investigated radio propagation within the 2.4 GHz ISM band, our literature study identified a scarcity of empirical research that specifically examines 2.4 GHz LoRa radio propagation.

III. Empirical Path Loss Models

A radio signal gets attenuated due to a path loss when propagating through a wireless medium. Fading and shadowing effects reduce the signal strength and introduce delays at the receiver. We define the path loss PL from the link budget as

$$PL(d) = P_t - P_r(d) - G_t(\theta) - G_r(\theta)\,, \tag{1}$$

where d is the distance between the transmitter and the receiver. The path loss accounts for the transmitted power P_t, the received power $P_r(d)$, and the misalignment from the maximum antenna gains, $G_t(\theta)$ and $G_r(\theta)$ at an angle θ.

A. Free Space Path Loss Model

The free-space path loss model concerns the omnidirectional propagation of a radio wave from a point source transmitter. At a receiver, positioned at the distance d from the transmitter, the loss of the radio signal is proportional to d/λ where $\lambda = c/f$ is the wavelength of the radio wave corresponding to the frequency f, and c is the speed of light. A first-order approximation considers a single direct path, with no reflected signal nor obstructions along the path. In this approximation, all the transmitted power directed through the antenna is effectively collected by the antenna aperture at the receiver. Based on this, the free space loss can be defined in decibels (dB) as [8]

$$PL_{\rm FS} = 92.45 + 20\log(f_{\rm GHz}) + 10n\log(d_{\rm km})\,, \tag{2}$$

where $f_{\rm GHz}$ is the frequency of the transmitting signal in GHz, $d_{\rm km}$ is the distance in kilometers, and n is the path loss exponent. In free space, the path loss follows an inverse square law described by a path loss exponents equal to $n = 2$.

B. Two-Ray Ground-Reflection Model

The two-ray ground-reflection model is used when a single ground reflection dominates the multipath effect for the propagating radio wave [21]. In this setting, the LOS component, modeled by the free-space path loss model, is superimposed by a reflected wave. The path loss of the two-ray ground-reflection model is defined as (in dB)

$$\begin{aligned} PL_{\rm TR} = {} & PL_{\rm FS} - 2G(\theta_{\rm LOS}) \\ & - 20\log|1 - \Gamma(\theta_{\rm ref})e^{-j\Delta\phi}|\,, \end{aligned} \tag{3}$$

where $PL_{\rm FS}$ is the free space path loss in dB as defined by Eq. (2). $G(\theta_{\rm LOS})$ is the antenna gain (assumed the same for both transmitter and receiver) evaluated at the angle $\theta_{\rm LOS}$ for the LOS direction and $\Gamma(\theta_{\rm ref})$ is the reflection coefficient of the ground. The reflection coefficient can be determined using a relative permittivity ε_g and for a vertically polarized ground-reflected wave at an angle $\theta_{\rm ref}$, and given as [13]

$$\Gamma(\theta_{\rm ref}) = \frac{-\epsilon_g \sin(\theta_{\rm ref}) + \sqrt{\epsilon_g - \cos^2(\theta_{\rm ref})}}{\epsilon_g \sin(\theta_{\rm ref}) + \sqrt{\epsilon_g - \cos^2(\theta_{\rm ref})}}\,. \tag{4}$$

Both $\theta_{\rm LOS}$ and $\theta_{\rm ref}$ can be determined from the geometry of the setup. The last factor is the phase difference between components that can be approximated as

$$\Delta\phi \approx \frac{4\pi h_t h_r}{\lambda d}\,, \tag{5}$$

where h_t and h_r are the transmitter and receiver antenna heights, respectively. The above approximation is valid when $d \gg (h_t + h_r)$. In the two-ray ground-reflection model, a break point d_b can be introduced as the distance from the transmitter where the ground-reflected wave and the direct wave cancel each other out i.e., $\Delta\phi = \pi$. In the far field, the break point can be calculated as $d_b = 4h_t h_r/\lambda$ [8], [21].

C. COST 231-Hata Model

The Hata propagation model is an empirical model based on data provided by Okumura and is valid over frequencies from $150 - 1500$ MHz therefore called the Okumura-Hata model [22]. The original model was later adjusted to address the frequency band of $1500 - 2000$ MHz hereafter referred to as the COST 231 extension or the COST 231-Hata model [23]. The model was built for network coverage prediction to be valid for for distances ranging from $1 - 20$ km with transmitter and receiver heights between 30 m and 200 m and between 1 m and 10 m, respectively.

The path loss of the COST 231-Hata model for the suburban and rural areas case is given by [23]

$$\begin{aligned} PL_{\mathrm{CH}} &= 46.3 + 33.9\log(f_{\mathrm{MHz}}) - 13.82\log(h_t) \\ &\quad - a(h_r, f_{\mathrm{MHz}}) + (44.9 - 6.55\log(h_t))\log(d_{\mathrm{km}}). \end{aligned} \tag{6}$$

The term $a(h_r, f_{\mathrm{MHz}})$ is a correction factor to account for the environment. For suburban and rural areas, it is given by [23]

$$\begin{aligned} a(h_r, f_{\mathrm{MHz}}) &= (1.1\log(f_{\mathrm{MHz}}) - 0.7)h_r \\ &\quad - (1.56\log(f_{\mathrm{MHz}}) - 0.8)\,. \end{aligned} \tag{7}$$

D. Walfisch-Bertoni Model

The Walfisch-Bertoni model considers diffraction from rooftops and buildings in a mobile communication system [24]. The model assumes that the propagating radio wave is scattered and arrives at the receiver with a reduced power. It is widely used as a first approximation for estimating the average path loss in areas with uniform building heights and spacing when predicting signal attenuation for mobile networks. We consider this model for our case of suburban area inspections, where we extrapolate to groups of vegetation (e.g., trees and bushes) with heights h_v and inter-vegetation distance d_v (Fig. 1). The transmitting antenna is positioned at

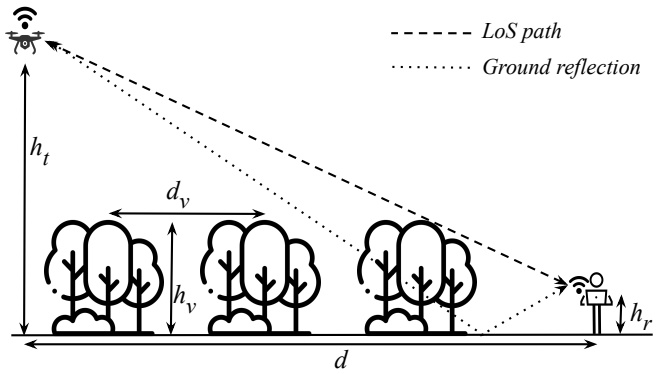

Fig. 1: Geometry for propagation models and the measurement setup. The scenario resembles the Walfisch-Bertoni model [24].

height $h_t - h_v$ above such obstacles and the receiver antenna is positioned at height h_r. Eq. (8) expresses the Walfisch-Bertoni path loss as a sum of the free space path loss and an excess loss factor L_{ex} resulting from scattered and diffracted waves

$$\begin{aligned} PL_{\mathrm{WB}} &= PL_{\mathrm{FS}} + L_{\mathrm{ex}}\,, \\ L_{\mathrm{ex}} &= 57.1 + A + \log(f_{\mathrm{MHz}}) \\ &\quad + 18\log(d_{\mathrm{km}}) - 18\log(h_t - h_v) \\ &\quad - 18\log\left(1 - \frac{d_{\mathrm{km}}^2}{17(h_t - h_v)}\right), \\ A &= 5\log\left(\left(\frac{d_v}{2}\right)^2 + (h_v - h_r)^2\right) \\ &\quad - 9\log(d_v) + 20\log\left(\arctan\left(\frac{h_v - h_r}{d_v}\right)\right). \end{aligned} \tag{8}$$

IV. Methodology

A set of measurements was obtained in the Mollerup forest in a suburban area near Aarhus, Denmark (Fig. 2). The area is characterized by countryside plains, low hills, and scarcely distributed sets of trees and bushes, that represent a typical area of low-density vegetation. Measurements for the different lengths were done in a straight line with a deviation of about 2%. The area is nearby a residential neighbourhood mainly populated with single-family houses. However, the line was not passing over the neighbourhood (cf. Fig 2).

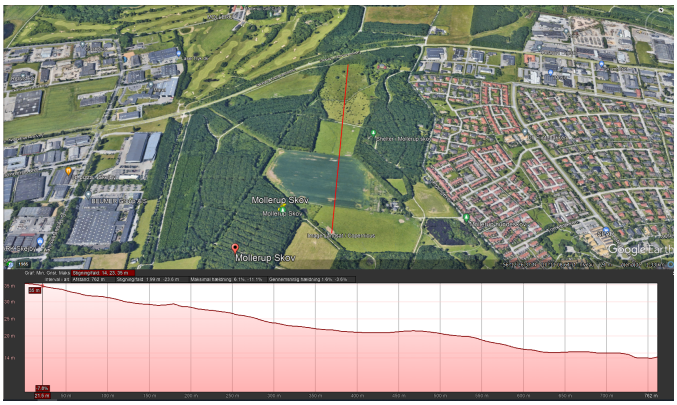

Fig. 2: Aerial photo of the test site (top) with a contour line for the example of an 800 m LOS experiment (bottom).

A. LoRa Module and UAV Setup

The LoRa module (Fig. 3a) is based on Semtech's SX1280 chipset for the radio interface [7]. It can be configured as either a transmitter or receiver. The LoRa transmitter is connected through the Serial Peripheral Interface (SPI) to a Raspberry Pi 4 companion computer mounted on a custom-built UAV (Fig. 3b). Telemetry messages are demodulated in a remote LoRa receiver connected through Universal Serial Bus (USB) to a laptop that is used for reception, storage, and post-processing of telemetry messages. The module uses an omnidirectional Inverted-F PCB antenna for communication. No special precautions have been made for placement of the modules during the tests. Data collection scripts have been made to carry out the measurement using the Host

(a) (b)

Fig. 3: (a) LoRa 2.4 GHz module stacked on a Raspberry Pi 4. The optional external antenna shown was not used in the experiments. (b) The UAV carrying the LoRa module.

Controller Interface (HCI) to control the LoRa communication system [7], [25]. We implemented a simplified Micro Air Vehicle Link (MAVLink) telemetry messages with flow control for our experiments [26]. The UAV carrying the LoRa module (Fig. 3b) is manually controlled by a pilot by using a proprietary radio controller (433 MHz) and monitored by a GCS (QGroundControl). An automated test program, written in Python, was used to seamlessly switch between different spreading factors while the UAV was in the air. The test program on the UAV was executed through a Secure Shell (SSH) connection using a WiFi hotspot.

B. Test Procedure

The UAV at height h_t reports telemetry data to a nearby ground station at a horizontal distance d and height h_r (cf. Fig. 1). Horizontal distances are estimated by using Google Maps. We further assume that the antenna radiation patterns of the transmitter and the receiver have characteristics similar to half-wavelength dipole antennas that are vertically oriented. The misalignment between antennas can therefore be approximated by $\theta = \tan^{-1}(\frac{h_t - h_r}{d})$.

For the path loss measurements, the UAV (transmitter) sends MAVLink messages continuously to a laptop (receiver) that logs messages including the reception statistics. Corresponding values for payload, RSSI, SNR, and CRC errors are recorded for further analysis. To obtain the RTT measurements, the laptop sends messages that require the receiver to respond with acknowledgments (ACK or NACK) of whether the transmissions were successful or not. The RTT timer is started right before the HCI message that requests the LoRa module to transmit a packet is sent. The timer is stopped as soon as the HCI message containing the ACK message is received. A window timer of 1000 ms is used to determine the time to wait before a packet is assumed to be lost. A transmit power of 13 dBm was used in the experiments.

V. Results and Discussion

From our experiments, we obtain RSSI and RTT measurements for various UAV heights and distances. We calculate the path loss based on RSSI measurements and compare these with the previously introduced path loss models.

A. Path Loss Study

For our scenarios, we considered $f = 2.4$ GHz, $d \in \{400, 800, 2400\}$ m, $h_t \in \{5, 10, 15, 20\}$ m, $h_r = 1.5$ m, omnidirectional antennas ($G(\theta) = 0$ dBi), and SF $\in \{7, 10, 12\}$. For the two-ray ground-reflecting model, we used $\varepsilon_g = 15$. For the Walfisch-Bertoni model, we use $h_v = 15$ m and $d_v = 30$ m. Figs. 4a-4c show the path loss for different heights of the UAV at three different distances. The path loss is calculated from the RSSI reported by the LoRa radio. A fixed spreading factor of SF = 7 was used in these experiments. The plots also show the path loss models introduced in Sec. III. A linear least square fitting is applied to deduce the path loss exponent for the measurements. In Table I, we summarize and compare our observations where we have also introduced the calculated break points [21].

For each model, the Root Mean Square Error (RMSE) is calculated using the mean value of the observations for the different lengths and heights of the UAV. Although none of the models provide an accurate description of our measurements, we find that the Walfisch-Bertoni model yields the closest fit with the lowest RMSE values in most scenarios. When the operating height is relatively low over long distances, the two-ray ground reflection model proves to be the most suitable fit. Only in one case is the COST 231-Hata model the closest fit (UAV height of 15 m at a distance of 400 m).

The remarkably low path loss exponents n observed in our experiment can be attributed to the advantageous LOS conditions at 2.4 km compared to the 800 m distance. At the latter range, the transmitted position stands at a height of 13 m above sea level, while the receiver is situated significantly higher at 35 m above sea level (cf. Fig. 2). These findings emphasize the critical role played by LOS in the path loss experiments.

B. Round Trip Time Experiments

We collected data for the RTT for different spreading factors: SF $\in \{7, 10, 12\}$. A bandwidth of 1625 kHz was used in the experiments. Only data for successful transmission were considered. The number of valid RTT measurement were in the range of 696 to 4648 data points. As expected, it can be observed that the symbol spread is dominating the RTT values of the A2G link and the differences in distance play an insignificant role. It is also noted that for SF $= 7$ and SF $= 10$, the requirement of a maximum latency of a one-way delay of 50 ms can be achieved when taking into account the asymmetry of the A2G link with 70.7% of the RTT spent for the outgoing packet (cf. Sec. V-C).

C. Goodput Experiment

An experiment was undertaken to determine the one-way goodput of the A2G communication channel. We designed a LoRa packet with a small amount of telemetry data is transmitted within a predefined period (Fig. 6). The experiments used a MAVlink frame of 40 bytes encapsulated with a 3-bytes *shim* header for encapsulating the MAVLink frame in the LoRa Packet Data Unit (PDU) [25]. LoRa uses a preamble,

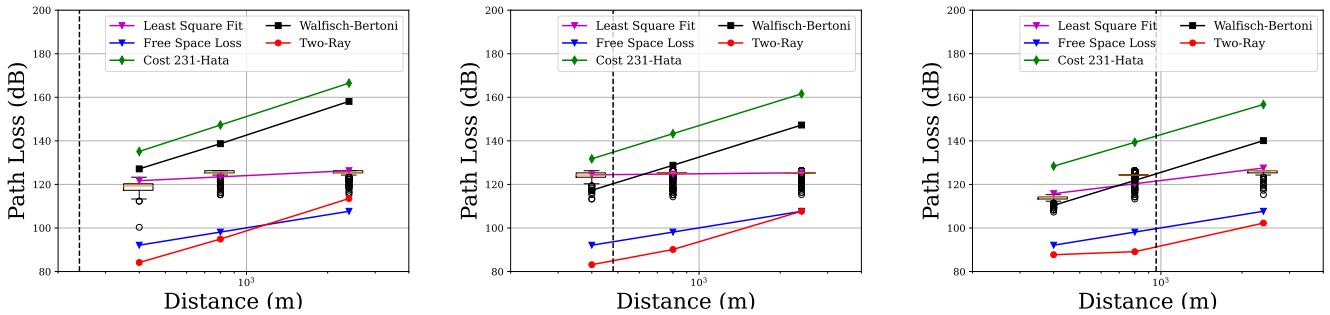

Fig. 4: Path loss for hovering heights $5, 10$, and 20 m, respectively. The break points are shown with dashed vertical lines.

TABLE I: RMSE values in dB and percentage (%) for the different considered models. Minima RMSE values are highlighted in **bold**. The receiver height $h_r = 1.5$ m in all cases. The parameters n and PL_0 result from the least square fitting.

h_t	d_b	d	N	Free-Space Loss		Cost 231-Hata		Walfisch-Bertoni		Two-Ray		Least square parameters	n	PL_0
5 m	240 m	400 m	529	26.98 dB	22.68%	16.38 dB	13.77%	**8.58 dB**	**7.21%**	34.89 dB	29.33%		0.59	106.28
		800 m	1119	27.50 dB	21.90%	21.70 dB	17.28%	**13.15 dB**	**10.47%**	30.70 dB	24.45%			
		2400 m	950	17.72 dB	14.14%	41.18 dB	32.85%	32.80 dB	26.17%	**11.87 dB**	**9.47%**			
10 m	480 m	400 m	747	32.43 dB	26.15%	9.66 dB	7.79%	**8.83 dB**	**7.12%**	41.26 dB	33.27%		0.12	121.21
		800 m	1109	27.12 dB	21.66%	18.16 dB	14.51%	**3.88 dB**	**3.10%**	35.11 dB	28.04%			
		2400 m	1090	17.57 dB	14.03%	36.44 dB	29.11%	22.12 dB	17.67%	**17.55 dB**	**14.01%**			
15 m	720 m	400 m	773	32.51 dB	26.09%	**5.33 dB**	**4.28%**	11.54 dB	9.26%	32.30 dB	25.92%		0.19	119.22
		800 m	1167	26.34 dB	21.17%	16.60 dB	13.34%	**1.32 dB**	**1.06%**	35.86 dB	28.82%			
		2400 m	843	18.31 dB	14.54%	32.82 dB	26.06%	**17.00 dB**	**13.50%**	21.54 dB	17.10%			
20 m	960 m	400 m	1488	21.84 dB	19.18%	14.52 dB	12.74%	**3.71 dB**	**3.26%**	26.22 dB	23.01%		1.51	76.4
		800 m	1150	26.15 dB	21.05%	15.16 dB	12.20%	**2.75 dB**	**2.21%**	35.14 dB	28.29%			
		2400 m	1057	18.25 dB	14.50%	30.81 dB	24.47%	**14.24 dB**	**11.31%**	23.26 dB	18.79%			

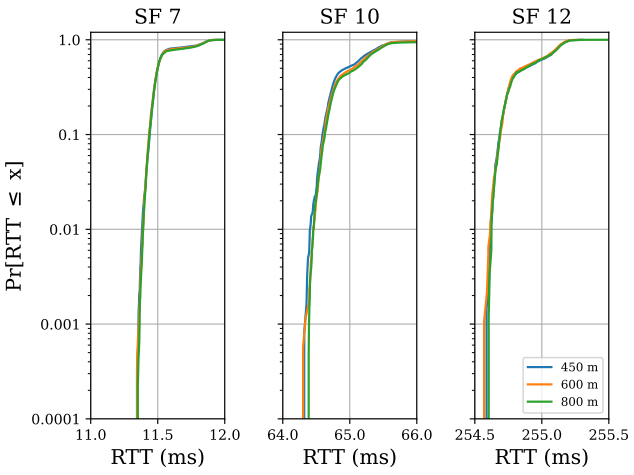

Fig. 5: RTT for all spreading factors and distances. The UAV height was 20 m in all cases.

5-byte header[1]. The default preamble size of 12 symbols with 4.25 symbol spacing was used. Converted into a coding rate equivalent of 4/5, this results in 20.3125 bytes. The LoRa ACK message is 3 bytes and it is sent in the LoRa PDU without MAVLink encapsulation. This means that when measuring the

[1]The LoRa PHY header encodes 8 symbols with a maximum coding rate of 4/8 [7], and a 2-byte CRC sum. This is equivalent to 5 bytes when converted to the coding rate of 4/5 used in our experiments.

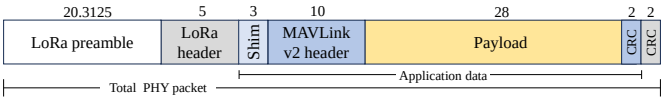

Fig. 6: Structure of LoRa packets used in the goodput experiments. Adapted from [7] and adjusted to the coding rate of 4/5.

RTT, 70.7% of medium access time is used for outgoing data and 29.3% of the time is for returning acknowledgments. By ignoring the packet processing time, which is much smaller than the transmission time, we can calculate the one-way goodput as the ration between the application data and the total number of transmitted bytes (Fig. 6).

Fig. 7 shows the data rates calculated from RTT measurements for different SFs. As expected, the observed goodput decreases as SF is increased. We compare with the upper limit for the LoRa radio at coding rate 4/5 and the same medium access time. Our values are 14.2%, 14.7% and 27.4% below the limit for the SFs 7,10 and 12, respectively. Furthermore, we can observe that the goodput in all cases is less than 60 kbps and cannot meet the requirements of a C2 channel. Nevertheless, we find that the link capacity is sufficient for telemetry as it satisfies the minimum required goodput rates for A2G communication [4]. Further, we find that an A2G communication channel based on 2.4 GHz LoRa is a good candidate for a secondary recovery channel as mandated by the EASA authority.

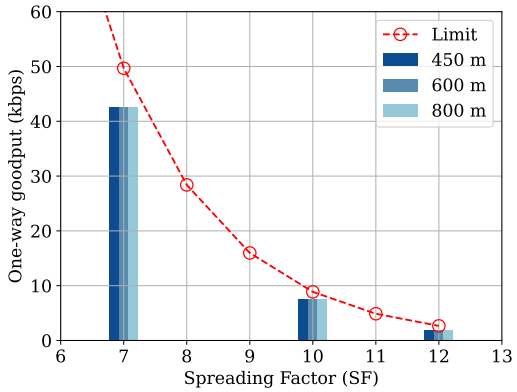

Fig. 7: Data rate of the LoRa 2.4 GHz link versus SF. The mean value of measurements is plotted. The Relative standard deviations are less than 1.21%.

VI. Conclusions

This study has presented results from an empirical study of A2G communication using LoRa in the 2.4 GHz ISM band based on the SX1280 LoRa radio from Semtech. Path loss, RTT, and goodput were determined from experiments conducted in a suburban area with a UAV at different hovering heights. This scenario is compatible with typical settings for civil infrastructure inspections. We have compared our results to a set of well-known path loss models and conclude that the Walfisch-Bertoni model fits our experimental observations best in most cases. In cases, where the operating height is relatively low at long distances, we find that the two-ray ground-reflection model provides the best fit. Overall, we conclude that 2.4 GHz LoRa has the potential for telemetry application in A2G communication. However, it can only partly satisfy the requirements of the C2 channel for UAV communications and only for lower spreading factors ($SF < 10$).

In the future, we will extend our study to more diverse environments and to expand our analysis to include interference and shadowing aspects.

Acknowledgments

This work was funded by the Innovation Fund Denmark project Drones4Energy with project number J. nr. 8057-00038A.

References

[1] E. Ebeid, R. Jacobsen, P. Schneider-Kamp, G. Vom Bögel, P. Guzzini, N. Luminari, C. Casarotti, M. Mandirola, D. Taurino, and A. Del Sole, "Autonomous Drones to Ensure Safety in Transport: Concept and Implementations," November 2022, SESAR Innovation Days. [Online]. Available: https://www.sesarju.eu/sesarinnovationdays

[2] S. G. Gupta, M. Ghonge, and P. M. Jawandhiya, "Review of Unmanned Aircraft System (UAS)," *International Journal of Advanced Research in Computer Engineering & Technology (IJARCET)*, vol. 2, no. 4, April 2013.

[3] EASA, "Opinion 01/2018: Unmanned aircraft system (UAS) operations in the 'open' and 'specific' categories," February 2018. [Online]. Available: https://www.easa.europa.eu/document-library/opinions/opinion-012018

[4] L. Shi, N. J. H. Marcano, and R. H. Jacobsen, "A Survey on Multi-unmanned Aerial Vehicle Communications for Autonomous Inspections," in *2019 22nd Euromicro Conference on Digital System Design (DSD)*, 2019, pp. 580–587.

[5] A. Augustin, J. Yi, T. Clausen, W. Townsley, A. Augustin, J. Yi, T. Clausen, and W. M. Townsley, "A Study of LoRa: Long Range & Low Power Networks for the Internet of Things," *Sensors*, vol. 16, no. 9, p. 1466, 2016.

[6] M. Saelens, J. Hoebeke, A. Shahid, and E. D. Poorter, "Impact of EU duty cycle and transmission power limitations for sub-GHz LPWAN SRDs: an overview and future challenges," *EURASIP Journal on Wireless Communications and Networking*, vol. 2019, pp. 1–32, 2019.

[7] Semtech, "Semtech SX128x Long Range Datasheet," July 2019, Data sheet, DS.SX1280-1-2.W.APP, Rev. 3.0.

[8] G. Callebaut and L. Van der Perre, "Characterization of LoRa Point-to-Point Path Loss: Measurement Campaigns and Modeling Considering Censored Data," *IEEE Internet of Things Journal*, vol. 7, no. 3, pp. 1910–1918, 2020.

[9] G. M. Bianco, R. Giuliano, G. Marrocco, F. Mazzenga, and A. Mejia-Aguilar, "LoRa System for Search and Rescue: Path-Loss Models and Procedures in Mountain Scenarios," *IEEE Internet of Things Journal*, vol. 8, no. 3, pp. 1985–1999, 2021.

[10] W. Khawaja, I. Guvenc, D. W. Matolak, U.-C. Fiebig, and N. Schneckenburger, "A Survey of Air-to-Ground Propagation Channel Modeling for Unmanned Aerial Vehicles," *IEEE Communications Surveys & Tutorials*, vol. 21, no. 3, pp. 2361–2391, 2019.

[11] N. Goddemeier and C. Wietfeld, "Investigation of Air-to-Air Channel Characteristics and a UAV Specific Extension to the Rice Model," in *2015 IEEE Globecom Workshops (GC Wkshps)*, 2015, pp. 1–5.

[12] N. Ahmed, S. S. Kanhere, and S. Jha, "On the importance of link characterization for aerial wireless sensor networks," *IEEE Communications Magazine*, vol. 54, no. 5, pp. 52–57, 2016.

[13] S. Kurt and B. Tavli, "Path-loss modeling for wireless sensor networks: A review of models and comparative evaluations," *IEEE Antennas and Propagation Magazine*, vol. 59, no. 1, pp. 18–37, 2017.

[14] Z. Zhang, S. Cao, and Y. Wang, "A long-range 2.4G network system and scheduling scheme for aquatic environmental monitoring," *Electronics (Switzerland)*, vol. 8, 2019.

[15] L. Polak and J. Milos, "Performance analysis of LoRa in the 2.4 GHz ISM band: coexistence issues with Wi-Fi," *Telecommunication Systems*, vol. 74, pp. 299–309, 2020.

[16] G. Chen, W. Dong, and J. Lv, "LoFi: Enabling 2.4 GHz LoRa and WiFi coexistence by detecting extremely weak signals," *Proceedings - IEEE INFOCOM*, vol. 2021-May, 2021.

[17] R. Falanji, M. Heusse, and A. Duda, "Range and Capacity of LoRa 2.4 GHz," in *International Conference on Mobile and Ubiquitous Systems: Computing, Networking, and Services*. Springer, 2022, pp. 403–421.

[18] T. Janssen, N. BniLam, M. Aernouts, R. Berkvens, and M. Weyn, "LoRa 2.4 GHz Communication Link and Range," *Sensors*, vol. 20, no. 16, 2020.

[19] F. Rander Andersen, K. Dilip Ballal, M. Nordal Petersen, and S. Ruepp, "Ranging Capabilities of LoRa 2.4 GHz," in *2020 IEEE 6th World Forum on Internet of Things (WF-IoT)*, 2020, pp. 1–5.

[20] F. Wolf, K. L. Deroff, S. de Rivaz, N. Deparis, F. Dehmas, and J.-P. Cances, "Benchmarking of narrowband lpwa physical layer ranging technologies," *2019 16th Workshop on Positioning, Navigation and Communications (WPNC)*, pp. 1–6, 2019.

[21] E. Zöchmann, K. Guan, and M. Rupp, "Two-ray models in mmwave communications," in *2017 IEEE 18th International Workshop on Signal Processing Advances in Wireless Communications*, 2017, pp. 1–5.

[22] M. Hata, "Empirical formula for propagation loss in land mobile radio services," *IEEE Transactions on Vehicular Technology*, vol. 29, no. 3, pp. 317–325, 1980.

[23] COST 231 Final Report, "Digital mobile radio towards future generation systems," 1999, chapter 4. [Online]. Available: http://www.lx.it.pt/cost231/final_report.htm

[24] J. Walfisch and H. Bertoni, "A theoretical model of UHF propagation in urban environments," *IEEE Transactions on Antennas and Propagation*, vol. 36, no. 12, pp. 1788–1796, 1988.

[25] Develco, "System Description," May 2020, Document no. DRO3191, Version 1.0.0.

[26] A. Koubâa, A. Allouch, M. Alajlan, Y. Javed, A. Belghith, and M. Khalgui, "Micro Air Vehicle Link (MAVlink) in a Nutshell: A Survey," *IEEE Access*, vol. 7, pp. 87 658–87 680, 2019.